Journal of Manufacturing Processes 56 (2020) 1088–1098

Contents lists available at ScienceDirect

Journal of Manufacturing Processes

journal homepage: www.elsevier.com/locate/manpro

Fluctuation effects in Wire Arc Additive Manufacturing of aluminium analysed by high-speed imaging

Tobias Hauser[a,c,*], Adrien Da Silva[a], Raven T. Reisch[b,c], Joerg Volpp[a], Tobias Kamps[c], Alexander F.H. Kaplan[a]

[a] Department of Engineering Sciences and Mathematics, Luleå University of Technology, S-971 87 Luleå, Sweden
[b] Chair of Robotics, Artificial Intelligence and Real-time Systems, Technical University of Munich, D-80333 Munich, Germany
[c] Corporate Technology, Siemens AG, D-81739 Munich, Germany

ARTICLE INFO

Keywords:
Direct Energy Deposition
Robotic
Laser arc

ABSTRACT

Wire Arc Additive Manufacturing is a near-net-shape processing technology which allows the cost-effective manufacturing of big and customized metal parts. In the present work the Wire Arc Additive Manufacturing of AW4043/AlSi5(wt.%) with different lead angles of the welding torch was investigated. It has been shown that for some lead angles fluctuation effects occur in the structures produced if the interlayer temperature is either too low or too high. All experiments were analysed by high-speed imaging whereby the welding phenomena could be observed. In the case of Wire Arc Additive Manufacturing with a lead angle above 10° at lower interlayer temperatures, the deposited track consists out of several, seperated WAAM globules and is no longer in a uniform track. In the case of the dragging and neutral Wire Arc Additive Manufacturing processes at higher interlayer temperatures, fluctuation effects occur. In addition, by evaluating the high-speed videos with computer vision, it was found that such fluctuation effects can be detected at the arc frequency of the process. To avoid fluctuation effects caused by too low or too high interlayer temperatures, a pushing Wire Arc Additive Manufacturing process with a slightly tilted lead angle should be used.

Introduction

Wire Arc Additive Manufacturing

Wire Arc Additive Manufacturing (WAAM) is a near-net-shape processing technology that is classified as one of the Direct Energy Deposition (DED) processes [1,2]. In WAAM, complex metal parts are produced layer by layer. The process is primarily intended for large and cost-effective components due to its high deposition rate compared to laserbased Additive Manufacturing processes [3]. The wire-based techniques are 2 to 50 times more cost efficient than powder-based techniques [1,2]. Currently most WAAM processes are based on Gas Metal Arc Welding, in particular the welding process Cold Metal Transfer (CMT) [4,5]. In the CMT process the wire is conveyed into the process zone via a pushing and pulling movement [4,6,7]. In one CMT cycle the wire is fed forward till the wire drops into the melt pool and an arc extinction occurs [4]. Afterwards the wire is mechanically pulled backward to split the wire from the melt pool and the CMT cycle starts again [4]. The CMT process enables a reduced thermal input and an improved stability of the arc which allows an accurate control of the deposited material [8]. The thermal state of the part directly influences the process stability and the resulting material properties [6,9,10]. Especially in WAAM any generated defects are closely related to the material and process parameters used [11]. The CMT process is affected by many different parameters such as voltage, current and wire feed speed [6]. Further parameters are the processing speed, the arc length correction, the dynamic correction, the type of shielding gas and many others [12–15]. For instance, an increase of the arc length correction results in a longer arc with increased arc energy which leads to a wider melt pool [16]. One parameter that affects the process stability, is the lead angle of the welding torch to the process zone which has previously been investigated for Gas Tungsten Arc Welding (GTAW) [17,18]. In GTAW the lead angle influences the width and the height of the deposited track [17]. With a larger angle to the vertical, the deposition width decreases and the deposition height increases [17]. Deep penetration of the deposited track can be achieved in laser welding [19]. Huang et al. found out that in hybrid welding, that combines the advantages of Gas Metal Arc Welding (GMAW) and laser welding, the laser should be in front of the wire to get a stable process [20].

* Corresponding author at: Department of Engineering Sciences and Mathematics, Luleå University of Technology, S-971 87 Luleå, Sweden.
E-mail addresses: tobias.hauser@ltu.se (T. Hauser), adrien.da.silva@ltu.se (A.D. Silva), raven.reisch@tum.de (R.T. Reisch), jorg.volpp@ltu.se (J. Volpp), tobias.kamps@siemens.com (T. Kamps), Alexander.Kaplan@ltu.se (A.F.H. Kaplan).

https://doi.org/10.1016/j.jmapro.2020.05.030
Received 26 March 2020; Received in revised form 29 April 2020; Accepted 20 May 2020
Available online 11 June 2020
1526-6125/ © 2020 The Author(s). Published by Elsevier Ltd on behalf of The Society of Manufacturing Engineers. This is an open access article under the CC BY license (http://creativecommons.org/licenses/BY/4.0/).

Materials in Wire Arc Additive Manufacturing

WAAM is possible with many different materials, but aluminium is of particular interest for large and customized lightweight components. Aluminium is widely used in different areas such as aerospace, ship building, train building and automotive industries because of its high-strength, light weight and high corrosion resistance [21–23]. WAAM has been recognized as one of the most efficient processing methods for individual, big and cost-effective structural parts [23–25]. As well as the ultra-pure aluminium, various alloyed aluminium materials are generally used. The most important alloying elements are copper, silicon, magnesium, zinc and manganese [12,26]. 4000 series aluminium alloys are typical for welding applications, making them suitable for Additive Manufacturing. Silicon (Si) is the main alloy component in the 4000 series [22]. Silicon reduces the melting point and improves the metal flow which leads to excellent weldability [22,27]. Köhler et al. performed WAAM for AlSi12(wt.%) and studied process characteristics, mechanical properties, and residual stresses [28]. Köhler et al. figured out that the solidification range and the WAAM settings such as arc length and pulse energy have significant effects on surface waviness [28]. They also suggested that a wide solidification range is more suitable for a smooth track [28]. Ortega et al. investigated WAAM of AlSi5(wt.%), a widely used welding alloy, and properties such as the microstructure of the resulting parts [4]. Ortega et al. found out that the width of the tracks increases layer by layer when building a wall due to heat accumulation if there is no break time between the layers [4]. Hackenhaar et al. investigated active cooling by an air jet in WAAM to prevent heat accumulation and concluded that this does not prevent an increase in substrate temperature, which shows that heat management is a major issue [29]. Wang et al. investigated the impact of arc current and arc pulse frequency on the porosity and grain structure for WAAM of AlSi5(wt.%) [30]. They found out that with increasing pulse frequency of the pulsed GTAW the grains become coarser and the porosity initially decreases and reaches its minimum at 50 Hz, but increases for higher frequencies due to the relationship between pore formation and gas escape [30]. Miao et al. investigated the microstructure and the mechanical properties of AlSi5(wt.%) manufactured by laser modified WAAM [31]. They found out that the additional energy input from the laser beam leads to a microstructure with finer grains and thus to increased mechanical properties [31].

Marangoni force

The humping phenomenon sometimes found in welding has also been studied in the context of WAAM [32,33]. One of the main driving forces of metal convection in the weld pool is the Marangoni force [34,35]. The Marangoni force is a surface tension force that is responsible for driving the flow of molten metal from the areas of low surface tension to the areas of high surface tension [33–35]. Mendez et al. created an arc force model using the static force balance theory [36]. The model assumes that humping occurs when the arc pressure exceeds the surface tension of the melt pool [36]. They concluded that the arc pressure model can describe the humping phenomenon [33]. However, what is not fully understood yet is the periodic behaviour of humping [33]. Li et al. and Huang et al. showed that high-speed imaging (HSI) is a suitable method to get a better insight into the process effects [37,38].

WAAM has great potential to be widely used in industry, but a lot of research still needs to be done to increase our understanding of the process, such as the influence of different lead angles in multi-layer processing. The object of the present work is multilayer processing using WAAM, considering the increasing interlayer temperatures and the related effects.

Material and Methods

Aluminium

The experiments were carried out with AW4043/AlSi5(wt.%) wire. Substrate plates of AW6061 with the dimensions 120 mm x 100 mm x 10 mm were used. The chemical compositions of the two alloys are shown in Table 1.

Table 1
Chemical composition of the aluminium alloys used in wt.% [31]

Alloy	Al	Si	Fe	Cu	Mn	Mg	Zn	Cr	Ti
AW4043	Bal.	4.5-6	0.8	0.3	0.05	0.05	0.1	-	0.2
AW6061	Bal.	0.4-0.8	0.7	0.15-0.4	0.15	0.8-1.2	0.25	0.04-0.35	0.15

Experimental set-up

The process set-up for WAAM consists of a motion control, a welding source, an industrial 6-axis robot, a worktable with substrate and an HSI system including a high-speed camera and an illumination laser. In order to measure the temperature during the process, thermocouples were attached to the substrate. Furthermore, a laser source is included in the WAAM cell for modifying the process by adding laser energy. The schematic set-up is shown in Fig. 1.

The equipment used for the experiments is shown in Fig. 2. In the experiments, a wall was built by processing 10 tracks on top of each other with a step height of 1.5 mm to 2.0 mm. The robot and the motion control used for WAAM are from ABB and the welding source with CMT functionality is from Fronius International. The fibre laser with a wavelength of 1064 nm and a maximum laser power of 8 kW is from IPG. High-speed videos of all experiments were made with the high-speed camera IDT NR4-S2 and the illumination laser CAVILUX HF.

Torch set-up of WAAM for different lead angles

For the first experiments, the lead angle was modified to investigate its influence on the melt pool and arc behaviour as well as on the geometry and porosity of the resulting WAAM parts. The schematic procedure is shown in Fig. 3.

The parameters used for WAAM with different lead angles are listed in Table 2. The lead angle was changed in a range of -10° to 40° in steps of 10°. All angles α are related to the vertical (Fig. 3). For positive lead angles α it is referred to as a pushing WAAM process, for negative lead angles it is a dragging WAAM process and for a vertical torch it is a neutral WAAM process. I.e. in the pushing WAAM processes, the wire is fed in the direction of travel and in the dragging WAAM processes, the wire is fed against the direction of travel. CMT mode 876 was used for processing, which is a specific mode of cold metal transfer and can be set in the Fronius welding source. The ROI (Region of Interest) is for all experiments in the middle part of the tracks and walls, since the ignition phase and shutdown phase of each single track differ regarding to the process parameters used.

Torch set-up of WAAM influenced by laser

Further experiments regarding the melt pool behaviour and the wetting of the substrate through higher preheating were made by adding laser energy to the WAAM process. The laser was used to simulate the increasing interlayer temperature during multi-layer processing. In the experimental set-up it was possible to influence the WAAM process by a fibre laser with a wavelength of 1064 nm and a laser power up to 8 kW. Aluminium has an absorption of 5% to 7% at a wavelength of 1064 nm. The laser is focused on the surface at a distance $d_{W\text{-}L}$ of 1.5 mm from the wire tip. The schematic procedure is shown in Fig. 4.

The parameters used for WAAM with added laser energy are listed in Table 3. The laser power was changed in a range of 0 W to 4500 W in steps of 1500 W. Due to the structure of the equipment used, the laser is inclined by 28° to the vertical.

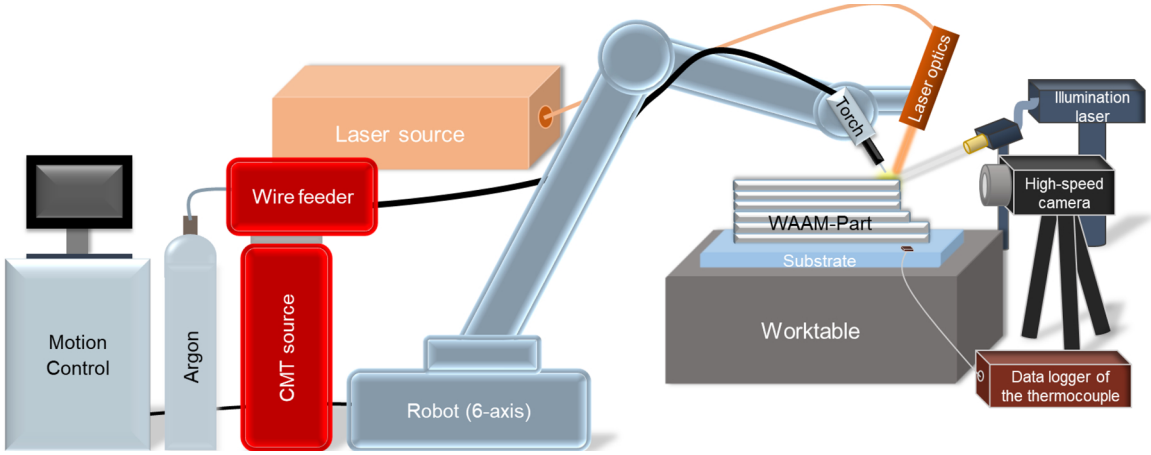

Fig. 1. Schematic experimental set-up of the robot based WAAM cell (Figure is for printing full size and in colour).

High-speed imaging system

For HSI of the process, the IDT NR4-S2 high-speed camera with a frame rate of 2000 frames per second and an exposure time of 3 µs was used. For HSI of such bright processes as WAAM, an illumination laser is used to illuminate the process at a specific wavelength, while all other process-related radiations outside the laser wavelength used are filtered to obtain a non-saturated view on the melt pool. In this case the illumination laser CAVILUX HF with a wavelength of 810 nm was used in combination with a band pass filter with a CWL (Central Wavelength) of 808 nm and FWHM (Full Width at Half Maximum) of 10 nm.

Analysis methods

All dimensions of the walls were measured with a caliper. The heights of the first and second track and the length of the melt pool were measured digitally in the high-speed videos. All high-speed videos of the walls manufactured with different lead angles were made in the second layer in the ROI. The high-speed videos of WAAM modified by adding laser energy were made in the first layer in the ROI. For measuring the temperature during WAAM of AlSi5(at.%) two thermocouples placed on the substrate as shown in Fig. 5 were used. In this thesis the interlayer temperature is one of the decisive factors. The temperature measurement by thermocouples will always differ from the actual interlayer temperature because the temperature was measured

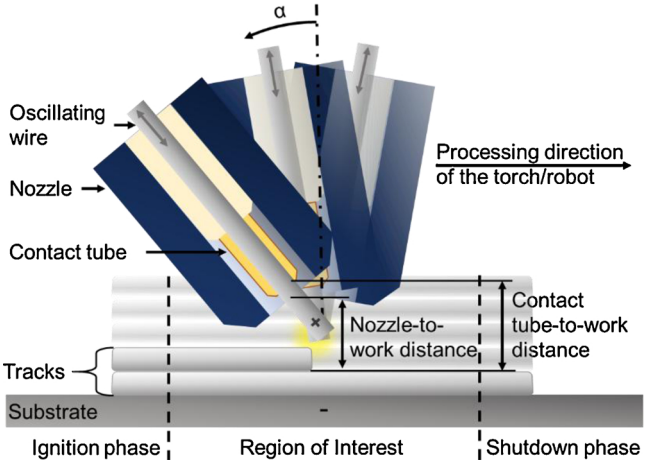

Fig. 3. Sketch of the modification of lead angles (Figure is for printing two-column format and in colour).

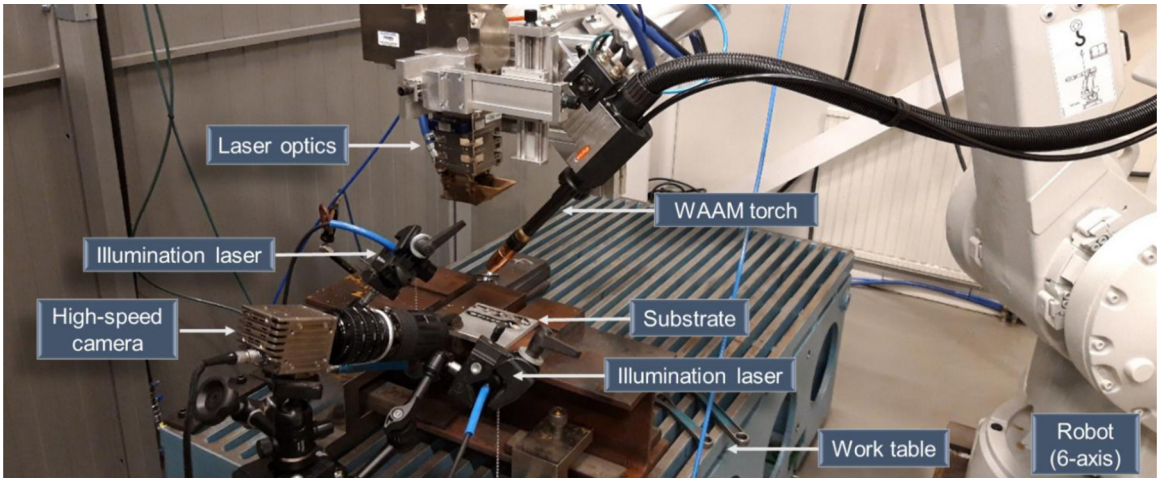

Fig. 2. Equipment for the robot-based Wire Arc Additive Manufacturing with HSI and the possibility of modifying the process by laser energy (Figure is for printing full size and in colour).

Table 2
Process parameters used for WAAM of AlSi5(wt.%) with modified lead angles

Parameter	Value
Material wire	AlSi5(wt.%)
Wire diameter	1.2 mm
Material substrate	AlSi1MgMn(wt.%)
Process mode	CMT mode 876
Ignition phase	10 mm
Region of Interest	80 mm
Shutdown phase	10 mm
Wire feed speed	4 m/min
Robot travel speed	0.6 m/min
Inert gas	18 l/min of Argon
Nozzle-to-work distance	10 mm
Contact tube-to-work distance	12 mm
Lead angle to vertical	−10°, 0°, 10°, 20°, 30°, 40°

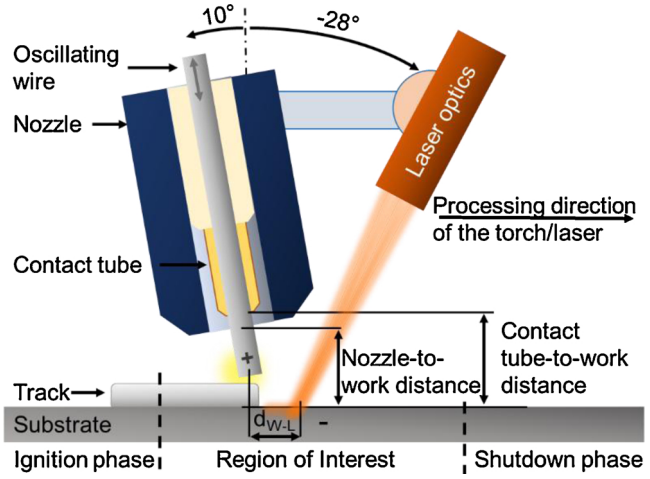

Fig. 4. Schematic set-up for preheating of the WAAM by adding laser energy (Figure is for printing two-column format and in colour).

Table 3
Parameters used for WAAM of AlSi5(wt.%) modified by a laser beam

Parameter	Value
Material wire	AlSi5(wt.%)
Wire diameter	1.2 mm
Material substrate	AlSi1MgMn(wt.%)
Process mode	CMT mode 876
Ignition phase	10 mm
Region of Interest	80 mm
Shutdown phase	10 mm
Wire feed speed	4 m/min
Robot travel speed	0.3 m/min
Inert gas	18 l/min of Argon
Nozzle-to-work distance	10 mm
Contact tube-to-work distance	12 mm
Lead angle	10°
Laser beam diameter	0.6 mm
Laser inclination	−28°
Focal length	250 mm
Laser irradiation-to-wire tip distance d_{W-L}	1.5 mm
Laser power	0 W to 4500 W

on the substrate and not directly on the surface of the last created layer. For this reason, the actual interlayer temperature will always be higher than the measured temperature, since the process-related energy input needs a certain time to be distributed over the entire component. Nevertheless, the measurements with thermocouples on the substrate should show reliable temperature values due to the high thermal conductivity of aluminium.

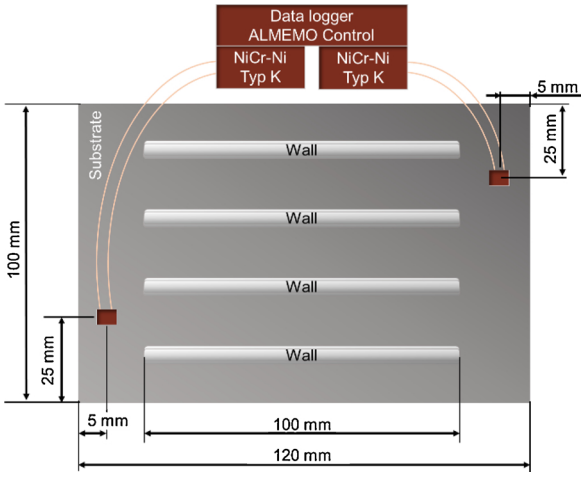

Fig. 5. Positioning of the thermocouples on the substrate during WAAM (Figure is for printing two-column format and in colour).

Computer vision

Computer vision algorithms in the programming environment 'Python' were used to analyse the high-speed videos of the experiments. The libraries cv2, argparse, matplotlib and numpy were imported for the algorithms. As a first step the high-speed videos were filtered through a Background Subtraction Method. The brightness threshold in the Background Subtraction Method is set to 800, which ensures that pixels with a brightness below this limit are displayed black and pixels with a brightness above this limit are displayed white. Afterwards the white pixels were counted, a time series of these white pixels was created and a Fast Fourier Transformation of this time series was performed. The diagram resulting from the Fast Fourier Transformation shows the normalized energy of the signal from the filtered high-speed video over the frequency. The absolute values of the diagrams from different high-speed videos cannot be compared with each other as the signal is highly influenced by the algorithms used. Only the relative values within a diagram can be compared with each other.

Results and Discussion

Melt pool behaviour at varied lead angles

Different lead angles in WAAM of AlSi5(wt.%) were analysed. 10 tracks of AlSi5(wt.%) were deposited in the z-direction for manufacturing a wall. The first tracks were produced with an Arc Length Correction of 20%, resulting in a wider melt pool and thus better wetting of the track on the substrate than without Arc Length Correction. All experiments regarding the varied lead angles were made without laser power. The resulting walls are shown in Fig. 6.

The high-speed images which represent one frame of the high-speed videos are shown in Fig. 7. In these high-speed images the wire feed direction is outlined through black dashed lines and the melt pool front is outlined through orange dashed lines. The processing direction is for all high-speed images the same.

The wall height, wall width and track height of the first and second layer as well as the melt pool length in the second layer are illustrated in Fig. 8. The deviations in the geometric dimensions and the fluctuation of the melt pool during processing are represented by error bars. Smaller error bars indicate more homogeneous geometrical dimensions or less fluctuation in the melt pool.

The most consistent behaviour for the height of the first track was achieved for WAAM with lead angles of -10° and 10°. After the first two layers, WAAM with lead angles of 20°, 30° and 40° showed at least twice as high deviation in the geometrical dimensions as WAAM with lead

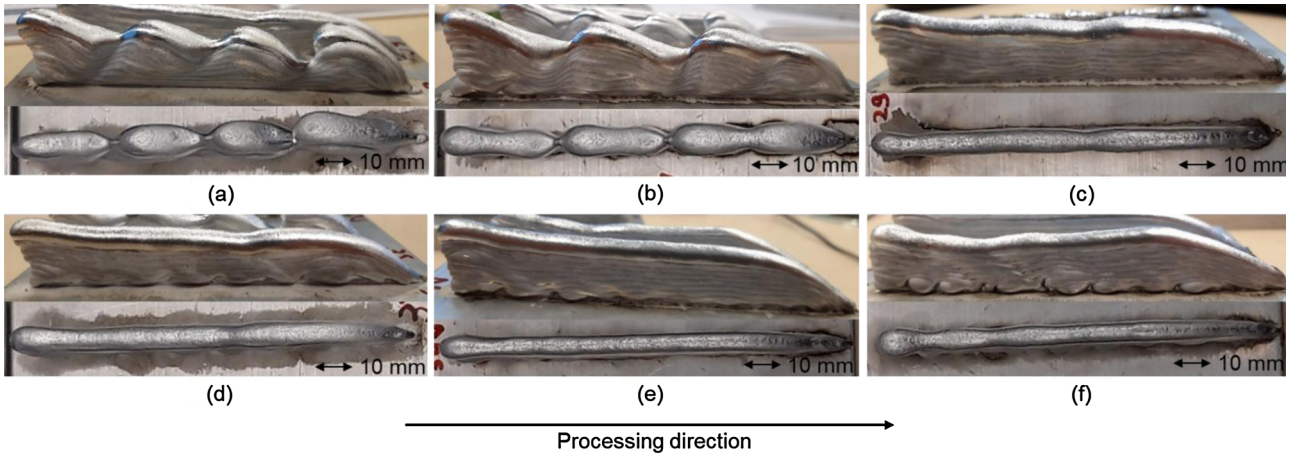

Fig. 6. Resulting walls with side view and top view for WAAM with lead angles of a) -10°, b) 0°, c) 10°, d) 20°, e) 30° and f) 40° (Figure is for printing full size and in colour).

angles of -10°, 0° or 10°. These deviations in the geometrical dimensions correlate with the melt pool fluctuations. For WAAM with a lead angle of 40° the deviations in the geometrical dimensions were even three times as high as for WAAM with lead angles of -10°, 0° or 10°. The melt pool length in the second layer decreases significantly with increasing lead angle from 10 mm for a lead angle of -10° to 7 mm for a lead angle of 30°. For WAAM with a lead angle of 40°, no stable melt pool was achieved in the first layers, as the high-speed images in Fig. 7 show. In addition, the melt pool fluctuations in z-direciton are higher for WAAM with lead angles of 20° and 40° what correlates with the high deviations in the geometrical dimensions of the first layers. For WAAM with a lead angle of 30°, the deviations of the geometrical dimensions appeared in the beginning of the track and then disappeared by the middle of the track. In the first layers a larger melt pool length correlates with a smaller fluctuation of the track height and smaller deviations in the geometrical dimensions, as shown in Fig. 8.

During the creation of the subsequent nine layers the behaviour of the melt pool changed for most of the experiments. In the walls manufactured at a lead angle of -10° and 0° the wall widths turned into a periodic pattern (Fig. 6a,b). In the pushing WAAM processes (Fig. 6c,d,e,f) such patterns did not occur in the final geometry. Even in WAAM with a lead angle of 40° the initial inhomogeneous track height in the first layers transformed over several layers into a wall without a fluctuating pattern. The reason for this shift is the rising temperature during manufacturing of the wall. For the whole process one parameter set with one specific wire feed speed and robot travel speed is set. So, during the whole process the deposited material and the energy input is the same. As the energy input through WAAM is higher than the energy output by convection and conduction, the whole sample including the substrate is heating up. At the beginning of the process the measured temperature is 22 °C (ambient temperature) and during the process the temperature rises from 60 °C after the first layer to 160 °C after the fifth layer and to 240 °C after the tenth layer as measurements with the thermcouples in Figure 9 show.

Due to the higher temperature in the upper layers, solidification of the melt pool takes longer, as the temperature gradient to the melting temperature of aluminium is lower compared to the first layers. Consequently the melt pool length increases and this leads to a uniform and smooth track in the pushing WAAM processes. For WAAM with pulling (lead angle of -10°) and vertical (0°) wire the increased melt pool length results in a wave pattern over the whole length of the wall, as shown in the wall height and wall width in Fig. 8.

WAAM effects at low temperatures

The WAAM effects which occur at room temperature without preheating are investigated in this chapter. Therefore the fluctuation of the track height in the first layer of WAAM with a lead angle of 40° was analysed in more detail in the high-speed images of Fig. 10. If the angle of the wire is too steep, the wire will form partial welding beads which will be called WAAM globules. These WAAM globules arise in WAAM for a lead angle of 20° and are clearly visible in WAAM for a lead angle

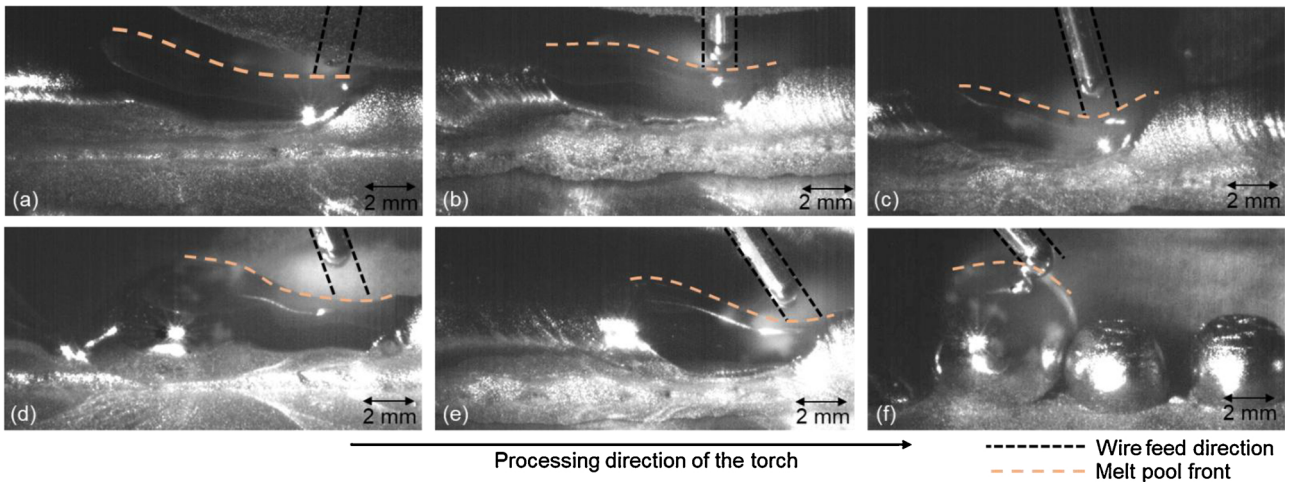

Fig. 7. High-speed images of WAAM with different lead angles of a) -10°, b) 0°, c) 10°, d) 20°, e) 30° and f) 40° (Figure is for printing full size).

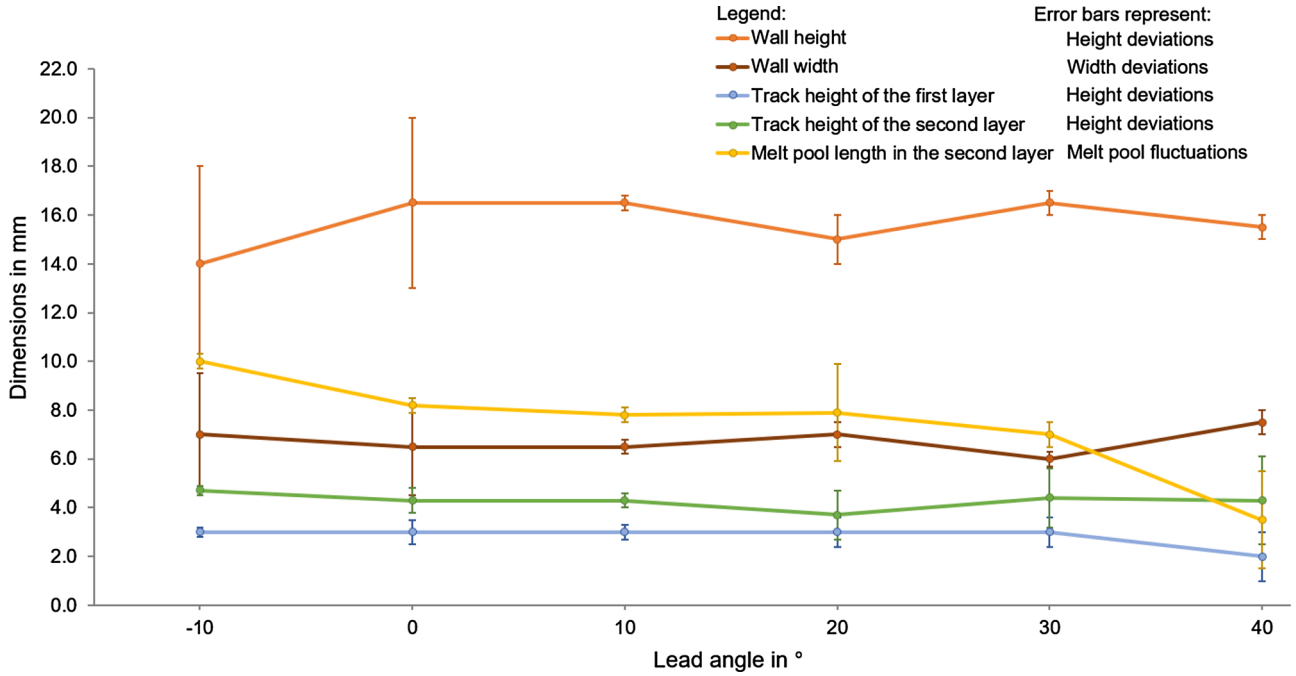

Fig. 8. Dimensions of the walls manufactured in WAAM for different lead angles without laser power (Figure is for printing full size and in colour).

of 40°. The formation of these WAAM globules is shown in Fig. 10.

The high-speed images in Fig. 10a show the progression of WAAM in the second layer of an aluminium wall over several CMT cycles. A lot of small WAAM globules were produced in the first layer of the wall, as shown in Fig. 10a. In the second layer these WAAM globules enlarge due to the dropping of the wire into the WAAM globules of the first layer, which is shown in CMT cycle N of Fig. 10a. The increasing temperature and enlarging WAAM globule lead to a merging of adjacent WAAM globules (I&II), which is shown in CMT cycle N + 11 of Fig. 10a. After the smaller WAAM globules have merged the marangoni force leads to a bulge of the resulting bigger WAAM globule (I&II), which is shown in the change between CMT cycle N + 11 and N + 12 of Fig. 10a. After the bulging of the WAAM globule (I&II) the wire can drop into the next WAAM globule (III), which is shown in CMT cycle N + 12 of Fig. 10a. For WAAM with a lead angle of 10° the material was deposited uniformly along the entire track as shown in Fig. 10b. The emerging effects for WAAM processes in the first layers with lead angles up to 10° and above 10° are illustrated in Fig. 11.

At the beginning of each experiment the substrate had a low temperature of 25 °C compared to the melting point of aluminium at 660 °C. In addition, aluminium has a high heat conductivity of 220 W/m*K which means that the heat is distributed very quickly throughout the entire component. This means that the deposited aluminium solidifies very quickly as shown in Fig. 10. At lead angles of less than 10° a uniform track is created but with lead angles above 10° the track is divided into several separated WAAM globules resulting in a nonuniform track as illustrated in Fig. 10. The fluctuation is more pronounced with a larger lead angle, as the wire is fed through the steeper angle over a longer period into the separated WAAM globules. As more layers are deposited the temperature increases throughout the component which leads to the disappearance of this effect over the layers, which is shown in the parts of Fig. 6d,e,f.

Arc behaviour at varied lead angles

The arc has a great influence on the resulting track geometries such

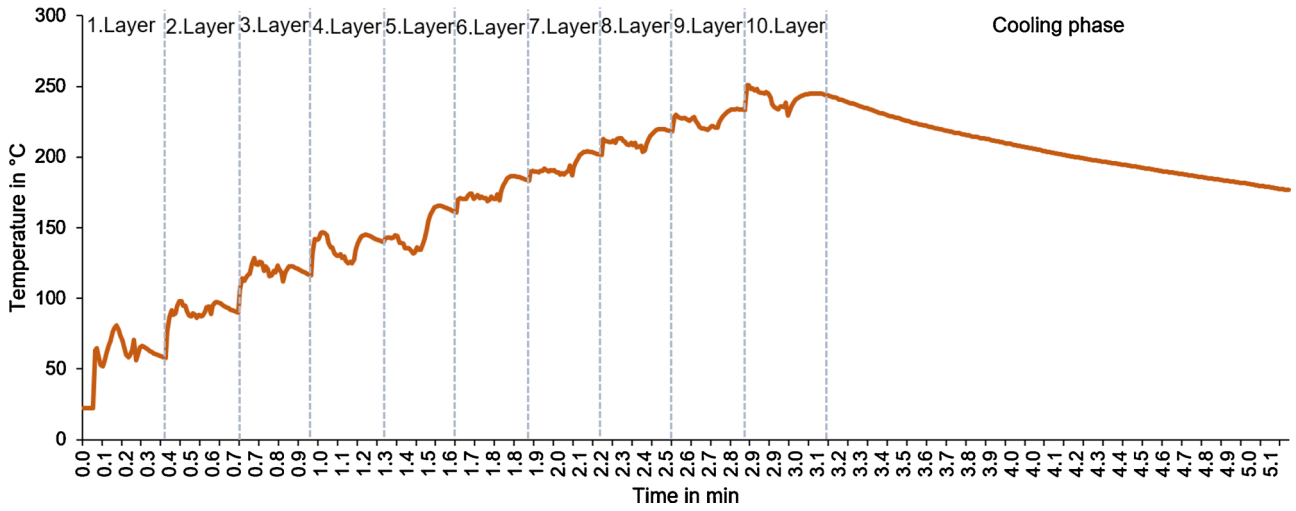

Fig. 9. Temperature curve during WAAM without laser power.

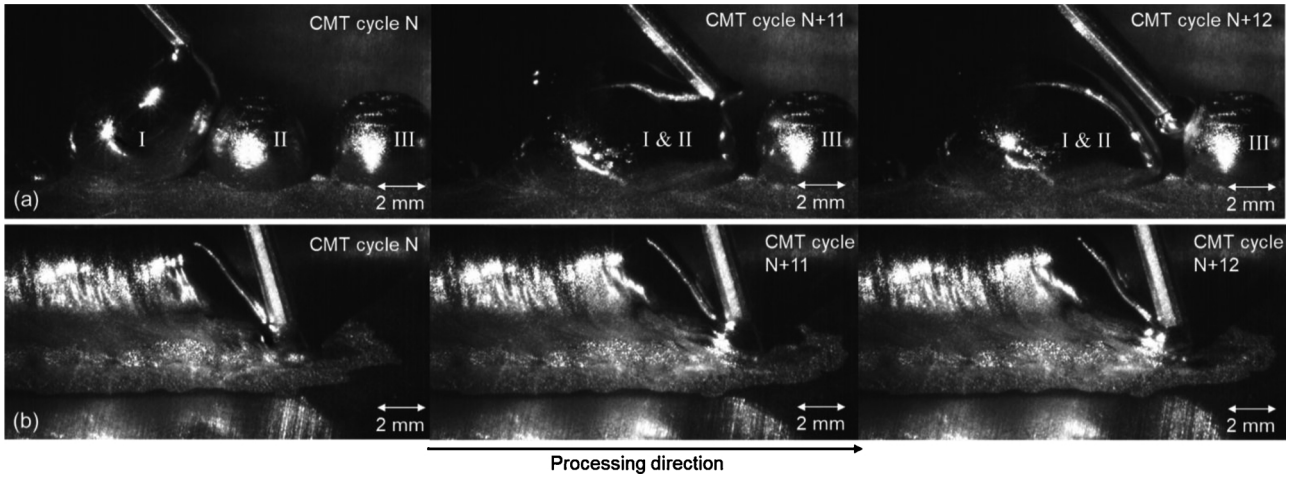

Fig. 10. High-speed images a) for WAAM with a lead angle of 40° in the second layer and b) for WAAM with a lead angle of 10° in the first layer (Figure is for printing full size).

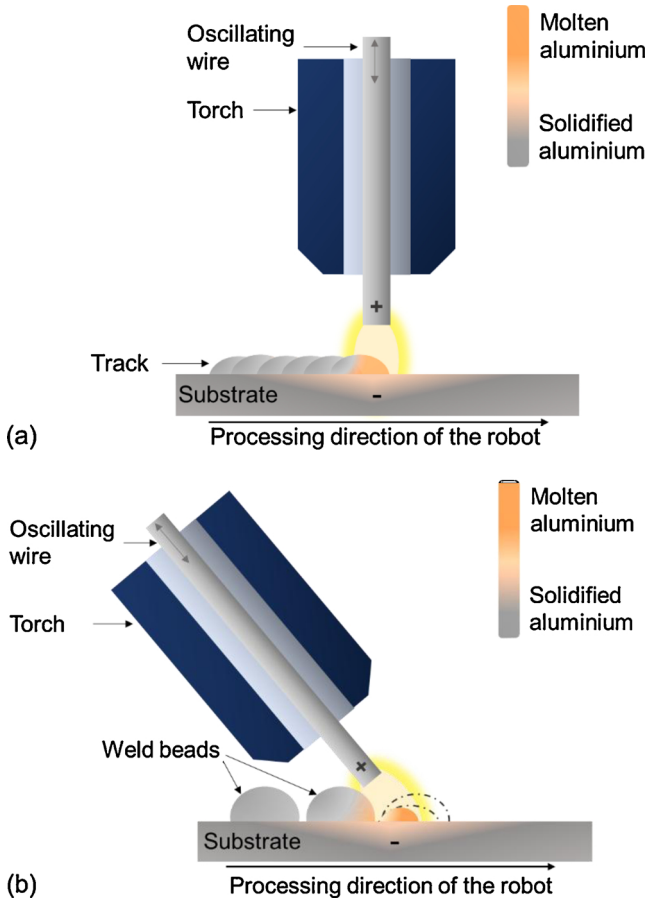

Fig. 11. WAAM effects occurring at low temperatures for the a) dragging and pushing WAAM processes with lead angles up to 10° and for the b) pushing WAAM processes with lead angles above 10° (Figure is for printing two-column format and in colour).

as the humping phenomenon described in the introduction and therefore the behaviour of the arc was analysed for all experiments. Computer vision algorithms were used to create binary filtered videos based on the high-speed videos. The moment the arc is ignited is shown in the high-speed images in Fig. 12 with the corresponding binary filtered images and the Area of Interest (AOI).

Through the binary filtered videos the time series of the arc can be analysed. Fast Fourier Transformations of these time series were generated in order to obtain the normalized energy of the signal for different frequencies of the arc. For stable processes maxima for 70 Hz to 80 Hz and their multiples should be visible because the CMT process works at this frequency and therefore the arc should also have this frequency. Computer vision was used to extract the current arc emissions in every image of the video. Based on that image preprocessing the normalized energy for frequencies up to 1000 Hz according to the Nyquist–Shannon sampling theorem can be calculated. The arc characteristics are shown in Fig. 13.

In Fig. 13 the arc characteristics for WAAM with lead angles of -10°, 0°, 10° and 30° are similar because they all have peaks in the green marked frequency intervals 75 Hz to 80 Hz, 150 Hz to 160 Hz, 225 Hz to 240 Hz, 300 Hz to 320 Hz and 375 Hz to 400 Hz. The peaks in these freqency modes are caused by the CMT process. For lead angles of 20° and 40° the signal is noisy because more oscillations occur. In the high-speed images of WAAM with different lead angles in Fig. 7 the fluctuation of the track height was detected only at lead angles of 20° and 40°, which also fits to the observation of the arc frequency. The noisy arc frequency signals of Fig. 13d,f result through the effect discussed earlier with reference to Fig. 10a. In the CMT cycle (N) of Fig. 10a, the wire drops into the track later than in CMT cycle (N + 12) of Fig. 8a resulting in a bigger stick-out of the wire and consequently in a time delay between the CMT cycles. This time delay is also shown in the noisy arc frequency signal of Fig. 13d,f.

WAAM effects at high temperatures

The WAAM effects which occur at higher interlayer temperatures caused by previous tracks are investigated in this chapter. For the pushing WAAM processes smooth tracks in the upper layers of the wall were created and no wave pattern did occur as shown in Fig. 6c,d,e,f. Even the cases in which no smooth tracks were initially created in the first layers due to the effect mentioned in Fig. 11b, smooth tracks were created in the upper layers.

For WAAM at a lead angle of 10°, experiments with additional preheating by different laser powers from 0 W to 4500 W were carried out to investigate the behaviour of pushing WAAM processes with increasing interlayer temperature. The experiments were carried out on

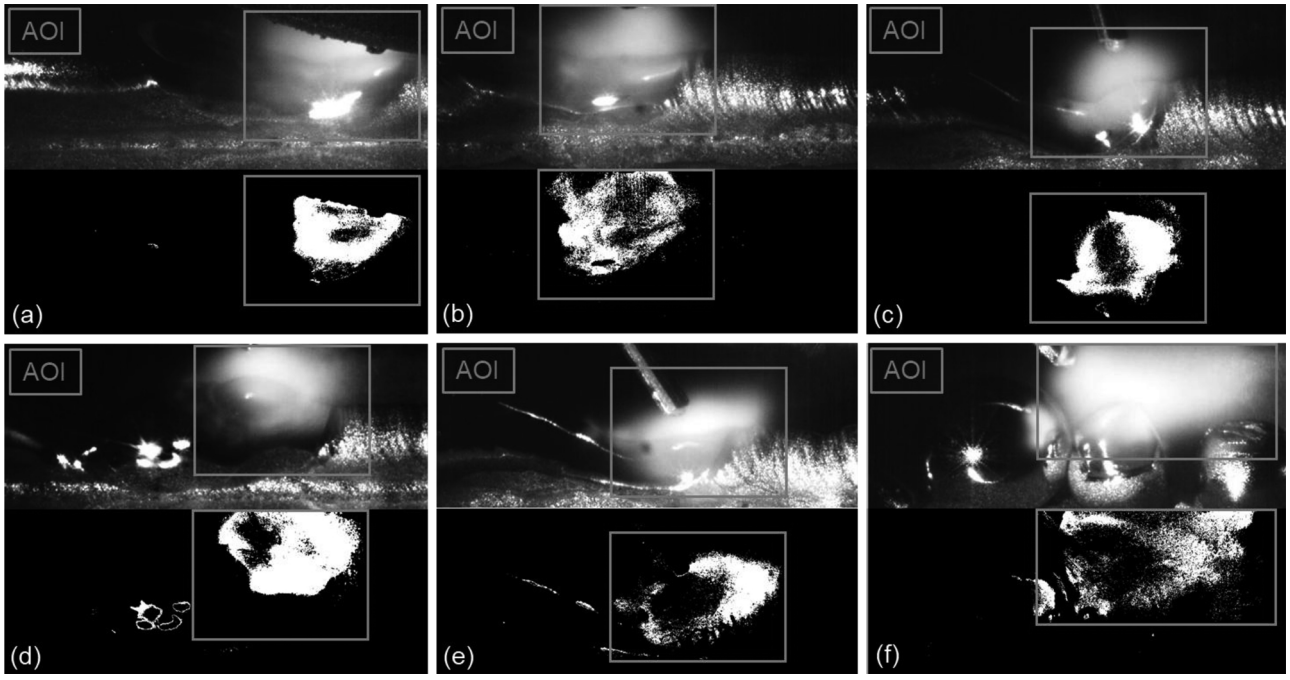

Fig. 12. High-speed images and corresponding binary filtered images for WAAM of AlSi5(wt.%) with different lead angles of a) -10°, b) 0°, c) 10°, d) 20°, e) 30° and f) 40° (Figure is for printing full size).

the substrate in order to avoid the influence of the unevenness of previous tracks. The laser was used because selective preheating is possible with the laser in order to simulate multi-layer processing on a preheated track. Through an increase in the laser power an increase in the interlayer temperature was simulated, as it would be the case in WAAM of a wall. The laser beam is marked orange and the melt pool front is drawn in white dashed lines in the high-speed images. The resulting tracks and high-speed images are shown in Fig. 14. The measured track height, track width and melt pool length are illustrated in Fig. 15.

The height decreases and the width increases with additional preheating, as the melt solidifies later for a higher preheating. The tracks with additional preheating trough a laser power of 3000 W or higher show a better wetting on the substrate than the tracks with a laser power below 3000 W. Based on an additional laser energy input, it can be determined that the melt pool length increases steadily with increasing laser power. The high-speed images also show how the melt pool front changes due to higher preheating. In the track without preheating the melt pool front is vertical to the substrate. With a preheating by a laser beam of 1500 W the melt pool flows slightly forward due to the higher interlayer temperature and the pushing WAAM process with a lead angle of 10°, which pushes the melt pool through the force transmitted by the oscillating wire and arc pressure pushes the melt in the processing direction as shown in Fig. 16a. For a laser power of 3000 W and 4500 W this effect is intensified. The same effect occurs when the component heats up over several layers as was the case in the experiments discussed in relation to Fig. 6 and illustrated in Fig. 16a.

For the dragging and neutral WAAM processes a wave pattern occurred at higher inerlayer temperatures as shown in Fig. 6a,b. These components show a wave pattern over the whole length of the geometry. The fluctuation of the geometries in the dragging and vertical WAAM processes started from the third layer with an interlayer temperature above 120 °C and intensified over the several layers. These wave patterns occurred due to the effect shown in Fig. 16b. As a result of the increasing interlayer temperature the melt pool stays molten for a longer period before it solidifies completely. In the neutral and dragging WAAM processes the melt pool is pushed against the processing direction by the oscillating wire and arc pressure which is shown in Fig. 16b. This results in an accumulation of material behind the process zone and increases until the force transmitted by the oscillating wire and the arc pressure is no longer sufficient to push the melt behind the process zone. As soon as this is the case a new material accumulation starts which finally ends in a wave pattern, as shown in Fig. 6a,b and illustrated in Fig. 16b.

The fluctuation effects in WAAM are therefore dependent on the lead angle and the interlayer temperature. In order to summarize the findings the interrelationships are shown graphically in Fig. 17. The graph clearly shows that the lead angle of 10° is most independent of the interlayer temperature, since no anomalies formed in this case.

Conclusions

- For WAAM with CMT mode at a lead angle above 10° the track results in separated WAAM globules and not in a uniform track. This effect is due to the low interlayer temperature, the low heat input in CMT mode and the high thermal conductivity of aluminium which causes the applied material to solidify very quickly. For a lead angle above 10° this leads to a bulging of the WAAM globules. The fluctuation is more pronounced with a larger lead angle, as the wire is fed through the steeper angle over a longer period into these bulging WAAM globules.
- The anomalies of the low temperature fluctuation of the track through bulging of WAAM globules can also be detected in the arc frequency. The noisy arc frequency signal in this case results from a time delay between the CMT cycles which is related to the fluctuation in the track as shown in the high-speed videos.
- Fluctuation effects also occur in the dragging and neutral WAAM processes at higher interlayer temperatures because the melt pool stays molten for a longer period and both the dragging and neutral

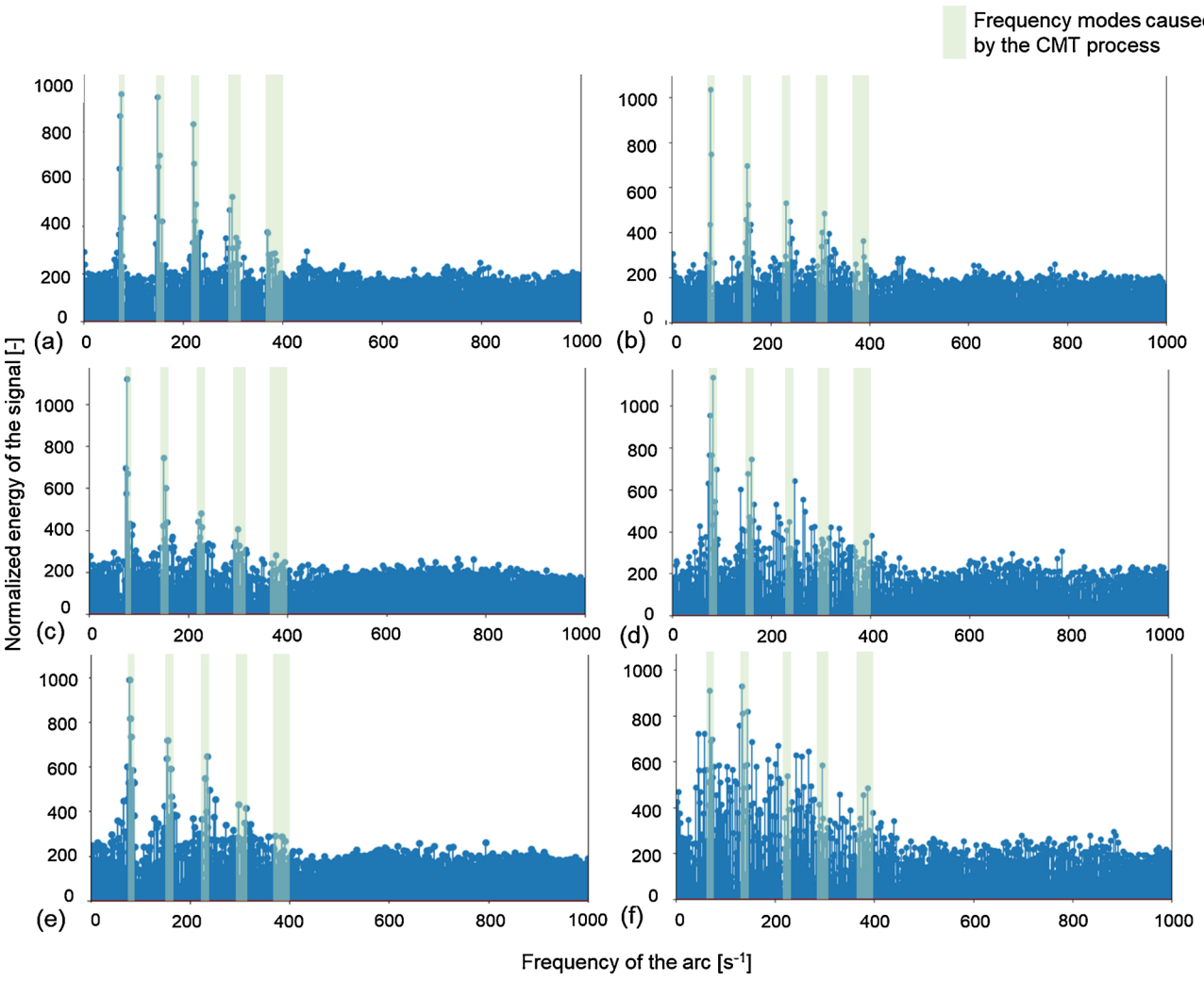

Fig. 13. Arc characteristics resulting from the Fast Fourier Transformations of the binary filtered high-speed videos for WAAM with lead angles of a) -10°, b) 0°, c) 10°, d) 20°, e) 30° and f) 40° (Figure is for printing full size and in colour).

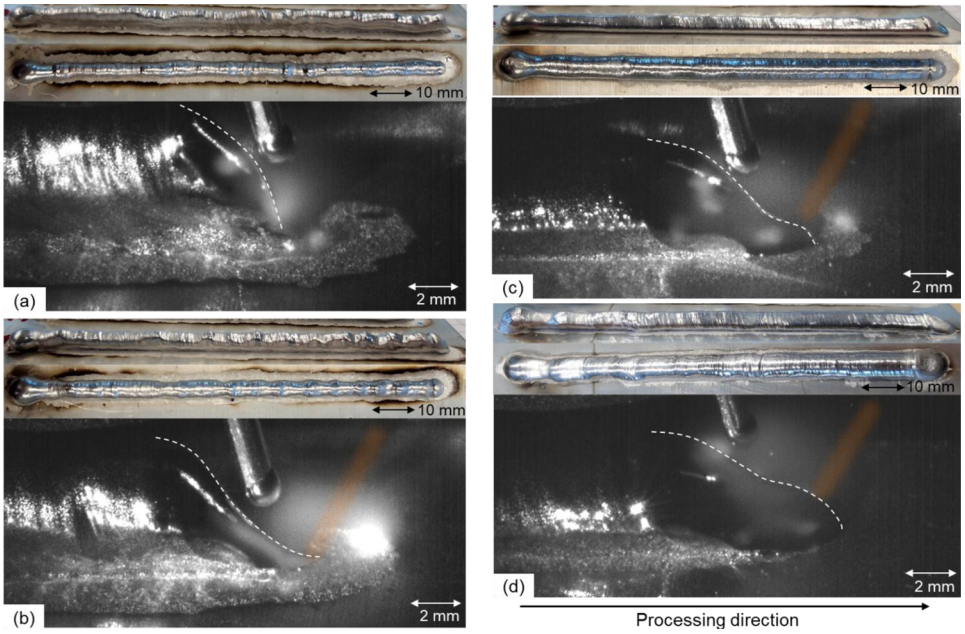

Fig. 14. Resulting tracks with side views, top views and corresponding high-speed images for WAAM with additional preheating by the (orange marked) laser beam with different laser powers of a) 0 W, b) 1500 W, c) 3000 W and d) 4500 W (Figure is for printing two-column format and in colour).

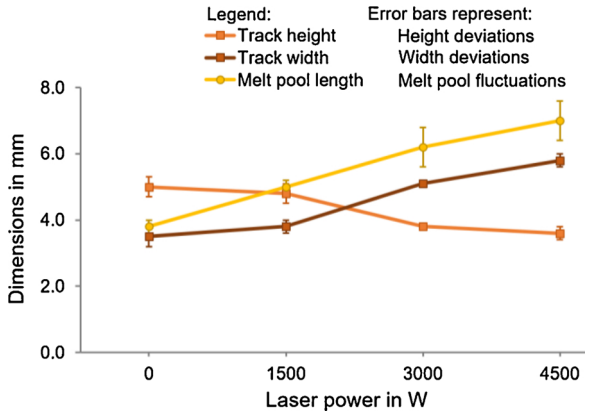

Fig. 15. Dimensions of the tracks for WAAM with additional preheating through different laser powers (Figure is for printing two-column format and in colour).

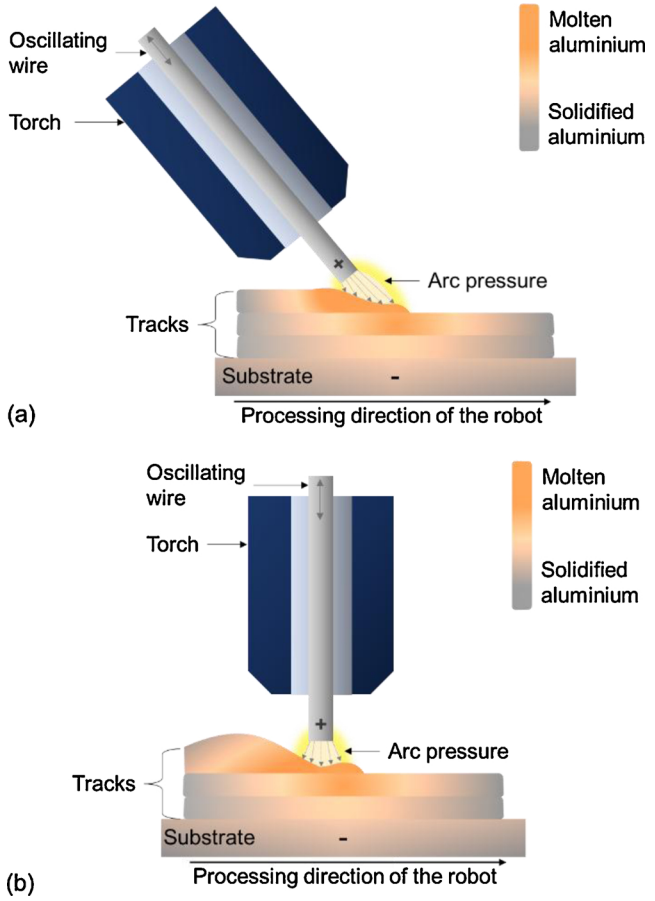

Fig. 16. WAAM effects occurring at high temperatures for the a) pushing WAAM processes and for the b) dragging and neutral WAAM processes (Figure is for printing two-column format and in colour).

WAAM processes push the melt pool against the processing direction by the oscillating wire and arc pressure, resulting in an accumulation of material after the process zone. This results in an accumulation of material behind the process zone which results in a wave pattern for a ten-layer wall. In the pushing WAAM processes no fluctuation effects occur at higher interlayer temperatures because the oscillating wire and arc pressure push the melt in the processing direction.

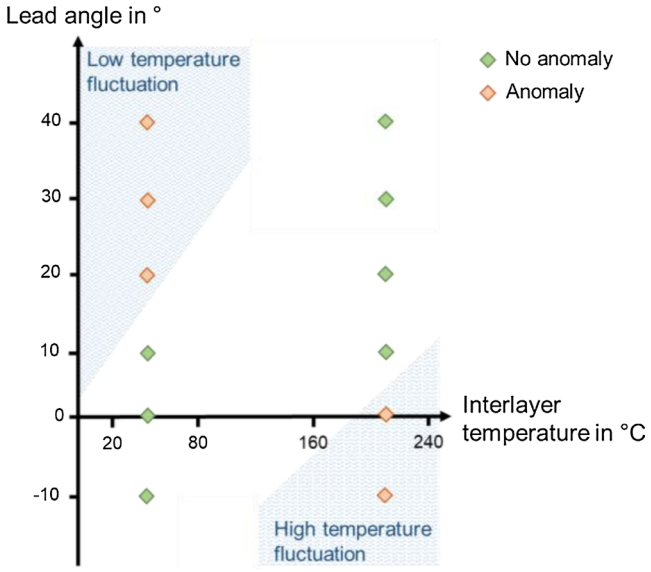

Fig. 17. WAAM effects for different interlayer temperatures and lead angles which occur for WAAM of AlSi5(wt.%) (Figure is for printing two-column format and in colour).

Declaration of Competing Interests

The authors declare that they have no known competing financial interests or personal relationships that could have appeared to influence the work reported in this paper.

Acknowledgement

The authors gratefully acknowledge funding from EIT RawMaterials for the project SAMOA - Sustainable Aluminium additive Manufacturing fOr high performance Applications, no. 18079.

References

[1] Derekar KS. A review of wire arc additive manufacturing and advances in wire arc additive manufacturing of aluminium. Materials Science and Technology 2018;34(8):895–916. https://doi.org/10.1080/02670836.2018.1455012.
[2] Thomas-Seale LEJ, Kirkman-Brown JC, Attallah MM, Espino DM, Shepherd DET. The barriers to the progression of additive manufacture: Perspectives from UK industry. International Journal of Production Economics 2018;198:104–18. https://doi.org/10.1016/j.ijpe.2018.02.003.
[3] DebRoy T, Wei HL, Zuback JS, Mukherjee T, Elmer JW, Milewski JO, et al. Additive manufacturing of metallic components – Process, structure and properties. Progress in Materials Science 2018;92:112–224. https://doi.org/10.1016/j.pmatsci.2017.10.001.
[4] Ortega AG, Corona Galvan L, Salem M, Moussaoui K, Segonds S, Rouquette S, et al. Characterisation of 4043 aluminium alloy deposits obtained by wire and arc additive manufacturing using a Cold Metal Transfer process. Science and Technology of Welding and Joining 2019;24(6):538–47. https://doi.org/10.1080/13621718.2018.1564986.
[5] Rodrigues TA, Duarte V, Miranda RM, Santos TG, Oliveira JP. Current Status and Perspectives on Wire and Arc Additive Manufacturing (WAAM). Materials (Basel) 2019;12(7). https://doi.org/10.3390/ma12071121.
[6] Zhou C, Wang H, Perry TA, Schroth JG. On the Analysis of Metal Droplets During Cold Metal Transfer. Procedia Manufacturing 2017;10:694–707. https://doi.org/10.1016/j.promfg.2017.07.024.
[7] Selvi S, Vishvaksenan A, Rajasekar E. Cold metal transfer (CMT) technology - An overview. Defence Technology 2018;14(1):28–44. https://doi.org/10.1016/j.dt.2017.08.002.
[8] Kazanas P, Deherkar P, Almeida P, Lockett H, Williams S. Fabrication of geometrical features using wire and arc additive manufacture. Proceedings of the Institution of Mechanical Engineers. Part B: Journal of Engineering Manufacture 2012;226(6):1042–51. https://doi.org/10.1177/0954405412437126.
[9] Wu B, Pan Z, van Duin S, Li H. Thermal Behavior in Wire Arc Additive Manufacturing: Characteristics, Effects and Control. In: Chen S, Zhang Y, Feng Z,

editors. Transactions on Intelligent Welding Manufacturing. Singapore: Singapore: Springer; 2019. p. 3–18.
[10] Wagiman A, Bin Wahab MS, Mohid Z, Mamat A. Effect of GMAW-CMT Heat Input on Weld Bead Profile Geometry for Freeform Fabrication of Aluminium Parts. AMM 2013;465-466:1370–4. https://doi.org/10.4028/www.scientific.net/AMM.465-466.1370.
[11] Wu B, Pan Z, Ding D, Cuiuri D, Li H, Xu J, et al. A review of the wire arc additive manufacturing of metals: properties, defects and quality improvement. Journal of Manufacturing Processes 2018;35:127–39. https://doi.org/10.1016/j.jmapro.2018.08.001.
[12] Dilthey U. Schweißtechnische Fertigungsverfahren 2: Verhalten der Werkstoffe beim Schweißen. 3rd ed. Berlin Heidelberg: Berlin, Heidelberg: Springer-Verlag; 2005.
[13] Williams SW, Martina F, Addison AC, Ding J, Pardal G. Colegrove P. Wire + Arc Additive Manufacturing. Materials Science and Technology 2016;32(7):641–7. https://doi.org/10.1179/1743284715Y.0000000073.
[14] González J, Rodríguez I, Prado-Cerqueira J-L, Diéguez JL, Pereira A. Additive manufacturing with GMAW welding and CMT technology. Procedia Manufacturing 2017;13:840–7. https://doi.org/10.1016/j.promfg.2017.09.189.
[15] Dinovitzer M, Chen X, Laliberte J, Huang X, Frei H. Effect of wire and arc additive manufacturing (WAAM) process parameters on bead geometry and microstructure. Additive Manufacturing 2019;26:138–46. https://doi.org/10.1016/j.addma.2018.12.013.
[16] Fronius International GmbH. TPS: Brief description of functions and settings. 2020.
[17] Gokhale NP, Kala P, Sharma V. Thin-walled metal deposition with GTAW welding-based additive manufacturing process. J Braz. Soc. Mech. Sci. Eng. 2019;41(12):641. https://doi.org/10.1007/s40430-019-2078-z.
[18] Silwal B, Walker J, West D. Hot-wire GTAW cladding: inconel 625 on 347 stainless steel. Int J Adv Manuf Technol 2019;102(9-12):3839–48. https://doi.org/10.1007/s00170-019-03448-0.
[19] Yu Y, Wang C, Hu X, Wang J, Yu S. Porosity in fiber laser formation of 5A06 aluminum alloy. J Mech Sci Technol 2010;24(5):1077–82. https://doi.org/10.1007/s12206-010-0309-4.
[20] Huang L, Wu D, Hua X, Liu S, Jiang Z, Li F, et al. Effect of the welding direction on the microstructural characterization in fiber laser-GMAW hybrid welding of 5083 aluminum alloy. Journal of Manufacturing Processes 2018;31:514–22. https://doi.org/10.1016/j.jmapro.2017.12.010.
[21] Kaibyshev R, Musin F, Lesuer DR, Nieh TG. Superplastic behavior of an Al–Mg alloy at elevated temperatures. Materials Science and Engineering: A 2003;342(1-2):169–77. https://doi.org/10.1016/S0921-5093(02)00276-9.
[22] Ostermann F. Anwendungstechnologie Aluminium. Berlin Heidelberg: Berlin/Heidelberg: Springer; 2014.
[23] Geng H, Li J, Xiong J, Lin X, Zhang F. Geometric Limitation and Tensile Properties of Wire and Arc Additive Manufacturing 5A06 Aluminum Alloy Parts. J. of Materi Eng and Perform 2017;26(2):621–9. https://doi.org/10.1007/s11665-016-2480-y.
[24] Wang F, Williams S, Colegrove P, Antonysamy AA. Microstructure and Mechanical Properties of Wire and Arc Additive Manufactured Ti-6Al-4V. Metall and Mat Trans A 2013;44(2):968–77. https://doi.org/10.1007/s11661-012-1444-6.
[25] Fang X, Zhang L, Chen G, Dang X, Huang K, Wang L, et al. Correlations between Microstructure Characteristics and Mechanical Properties in 5183 Aluminium Alloy Fabricated by Wire-Arc Additive Manufacturing with Different Arc Modes. Materials (Basel) 2018;11(11). https://doi.org/10.3390/ma11112075.
[26] Le Zhou Hyer H, Park S, Pan H, Bai Y, Rice KP, et al. Microstructure and mechanical properties of Zr-modified aluminum alloy 5083 manufactured by laser powder bed fusion. Additive Manufacturing 2019;28:485–96. https://doi.org/10.1016/j.addma.2019.05.027.
[27] Yang Q, Xia C, Deng Y, Li X, Wang H. Microstructure and Mechanical Properties of AlSi7Mg0.6 Aluminum Alloy Fabricated by Wire and Arc Additive Manufacturing Based on Cold Metal Transfer (WAAM-CMT). Materials (Basel) 2019;12(16). https://doi.org/10.3390/ma12162525.
[28] Köhler M, Fiebig S, Hensel J, Dilger K. Wire and Arc Additive Manufacturing of Aluminum Components. Metals 2019;9(5):608. https://doi.org/10.3390/met9050608.
[29] Hackenhaar W, Mazzaferro JAE, Montevecchi F, Campatelli G. An experimental-numerical study of active cooling in wire arc additive manufacturing. Journal of Manufacturing Processes 2020;52:58–65. https://doi.org/10.1016/j.jmapro.2020.01.051.
[30] Wang D, Lu J, Tang S, Yu L, Fan H, Ji L, et al. Reducing Porosity and Refining Grains for Arc Additive Manufacturing Aluminum Alloy by Adjusting Arc Pulse Frequency and Current. Materials (Basel) 2018;11(8). https://doi.org/10.3390/ma11081344.
[31] Miao Q, Wu D, Chai D, Zhan Y, Bi G, Niu F, et al. Comparative study of microstructure evaluation and mechanical properties of 4043 aluminum alloy fabricated by wire-based additive manufacturing. Materials & Design 2020;186:108205https://doi.org/10.1016/j.matdes.2019.108205.
[32] Nguyen TC, Weckman DC, Johnson DA, Kerr HW. High speed fusion weld bead defects. Science and Technology of Welding and Joining 2006;11(6):618–33. https://doi.org/10.1179/174329306X128464.
[33] Yuan L, Pan Z, Ding D, He F, van Duin S, Li H, et al. Investigation of humping phenomenon for the multi-directional robotic wire and arc additive manufacturing. Robotics and Computer-Integrated Manufacturing 2020;63:101916https://doi.org/10.1016/j.rcim.2019.101916.
[34] Kou S, Limmaneevichitr C, Wei P. Oscillatory Marangoni Flow: A Fundamental Study by Conduction-Mode Laser Spot Welding: Through Marangoni flow, a surface-active agent can affect not only the weld pool depth, but also the pool surface deformation, pool surface oscillation, and ripple formation. THE WELDING JOURNAL 2011;90:229–40.
[35] Ahsan MRU, Cheepu M, Ashiri R, Kim T-H, Jeong C, Park Y-D. Mechanisms of weld pool flow and slag formation location in cold metal transfer (CMT) gas metal arc welding (GMAW). Weld World 2017;61(6):1275–85. https://doi.org/10.1007/s40194-017-0489-y.
[36] Humping Formation in High Current GTA Welding. In: Mendez Patricio F, Niece Krista L, Eagar Thomas W, editors. proceedings of the International Conference on Joining of Advanced and Speciality Materials II. 1999.
[37] Huang J, Yuan W, Yu S, Zhang L, Yu X, Fan D. Droplet transfer behavior in bypass-coupled wire arc additive manufacturing. Journal of Manufacturing Processes 2020;49:397–412. https://doi.org/10.1016/j.jmapro.2019.12.002.
[38] Li Y, Yu S, Chen Y, Yu R, Shi Y. Wire and arc additive manufacturing of aluminum alloy lattice structure. Journal of Manufacturing Processes 2020;50:510–9. https://doi.org/10.1016/j.jmapro.2019.12.049.

Tobias Hauser was born in Ulm, Germany in 1995. He graduated in mechanical engineering at the Friedrich Alexander university Erlangen-Nuremberg (FAU) with a Master of Science. Since January 2019, he is working on his PhD in the fields of Laser Metal Deposition and Wire Arc Additive Manufacturing at the chair of Manufacturing Systems Engineering at Luleå University of Technology, Sweden.

Adrien Da Silva is a PhD student at Luleå University of Technology, Sweden, within the group Manufacturing Systems Engineering. He graduated in 2018 from Icam engineering school in Toulouse, France. His thesis' subject is laser beam-material interactions in Additive Manufacturing, with a focus on aluminium alloys.

Raven T. Reisch graduated in mechatronics and information technology as well as in mechanical engineering at the Technical University of Munich (TUM) with a Master of Science. Since 2019, he is working on his PhD in the area of context sensitive monitoring systems in Wire-Arc-Additive-Manufacturing at the chair of Robotics, Artificial Intelligence and Embedded Systems at TUM under the supervision of Professor Knoll.

Dr.-Ing. Jörg Volpp studied in Stuttgart (Germany). During his studies, he worked for the IFSW in Stuttgart and as an intern for Bosch GmbH in Charleston, SC (USA). He finished his diploma thesis at Bosch GmbH, Schwieberdingen (Germany) in 2011 in the field of laser welding of steels. From 2011 till 2017, he worked for BIAS GmbH in Bremen (Germany) in the field of laser deep penetration welding and received his PhD in 2017. Since June 2017, he works in the Laser group at Luleå University of Technology (Sweden).

Dr.-Ing. Tobias Kamps has graduated from RWTH Aachen University, Germany and Tsinghua University, Beijing, P.R. of China with a degree in Industrial Engineering. In parallel he worked at MTU Aero Engines, Munich, Germany as well as at Fraunhofer ILT, Aachen, Germany and Laboratory for Machine Tools and Production Engineering (WZL), Aachen, Germany on topics of Additive Manufacturing and high-performance machining processes. After completing his PhD work at Fraunhofer IGCV, Augsburg, Germany and MIT, Cambridge, MA, USA on Process Development and Industrialization of Additive Manufacturing, he joined Siemens, Munich, Germany for working on digitalization of production systems.

Prof. Alexander Kaplan was born in Vienna, Austria in 1967. He was employed as researcher at Vienna University of Technology from 1989 to 2000. In 1994 he received his PhD-degree on the modelling of laser welding. After a post-doc year at Osaka University, Japan, from 2002 on he has been appointed as professor and chair of Manufacturing Systems Engineering at Luleå University of Technology, Sweden. Alexander Kaplan has particular experience in mathematical modelling and high speed imaging of laser materials processing, particularly for laser welding, laser cutting and laser additive manufacturing.